nature communications

Article

https://doi.org/10.1038/s41467-026-68341-3

Earthquakes act as a capacitor for terrestrial organic carbon

Received: 29 June 2025

Accepted: 30 December 2025

Published online: 23 January 2026

Check for updates

Jie Liu[1,2], Xuanmei Fan[1] ✉, Tristram Hales[2], Erin L. Harvey[3], A. Joshua West[4], John D. Jansen[5], Xiaolu Tang[1,6,7] & Qiang Xu[1]

Earthquakes and seismically-induced landslides accelerate carbon export from mountains by eroding hillslope soil carbon. However, a quantitative understanding of their net contribution to carbon cycling remains incomplete. Using the 2008 M_w 7.9 Wenchuan Earthquake which generated the largest landslide volume in recent history, we quantify its carbon mass balance accounting for storage, loss, and transport within the ensuing sediment cascade. Thanks to post-event revegetation and extensive intermontane sediment storage, we show that the earthquake boosted Longmenshan carbon mass by ~10%. Given the stability of these deposits and low rates of carbon export, we anticipate this landslide carbon will persist for centuries to millennia before gradually declining. In effect, we demonstrate that earthquakes and landslides function as capacitors, regulating carbon storage and discharge across mountain belts over time. This suggests frequent landslides in seismically-active mountains may lead to a net carbon sequestration, providing a critical and direct link between tectonics and the carbon cycle.

Large earthquakes play a dual role in the terrestrial organic carbon system: they emit carbon to the atmosphere by destroying vegetation that subsequently decays[1,2], and they store particulate organic carbon in the ensuing sediment cascade[3–5]. Landslides (hereafter explicitly coseismic) are the main players perturbing the carbon mass balance of a mountain belt during and following an earthquake. Organic carbon eroded by landslides can take a number of pathways through mountain catchments; some fraction is stored on hillslopes and in headwater channels, while the rest is exported via drainage networks and carried ultimately into long-term sinks[6–8]. The amount of carbon temporarily stored in these landslide deposits, and the timescale over which it is released and exported, effectively act as a "carbon capacitor", buffering the interval between carbon production and its eventual transfer downstream. While erosion of petrogenic (i.e., rock-derived) organic carbon also plays an important role in the long-term carbon cycle[9], our focus here is on the larger fluxes associated with production, burial, and loss of terrestrial organic carbon (hereafter explicitly OC) within mountain belts following large earthquakes.

The largest continental earthquakes generate up to ~ 50 km^3 of landslide deposits composed of soil and fragmented rock[10]. These earthquake-triggered slope failures entrain soil OC and live biomass, creating an OC store whose magnitude over time depends on the volume of landslide deposits and the rate at which they are eroded[11]. Such deposits largely rest on hillslopes, where typically less than 10% are eroded immediately after the earthquake, while the majority remain stable for hundreds or even thousands of years[12–16]. The rate of sediment and OC export is a function of the density of the newly developed drainage network on the landslide itself, together with its connectivity to the river below[17,18] and the efficiency of hillslope erosion processes such as debris flows[12]. Where this connectivity has been measured, for instance following the Chi-Chi, Wenchuan and Gorkha earthquakes, 5–60% of landslides are shown to be connected to a

[1]State Key Laboratory of Geohazard Prevention and Geoenvironment Protection, Chengdu University of Technology, Chengdu, China. [2]School of Earth and Environmental Sciences, Cardiff University, Main Building, Park Place, Cardiff, UK. [3]Department of Geography, Durham University, Durham, UK. [4]Department of Earth Sciences, University of Southern California, Los Angeles, CA, USA. [5]GFÚ Institute of Geophysics, Czech Academy of Sciences, Prague, Czechia. [6]College of Ecology and Environment, Chengdu University of Technology, Chengdu, China. [7]Tianfu Yongxing Laboratory, Chengdu, China.
✉e-mail: fxm_cdut@qq.com

drainage network[19], though erosion is likely to be less efficient in the smallest headwater channels[20]. The highest post-event sediment yields measured historically are reported from the 1970 Madang Earthquake (Papua New Guinea), where up to 50% of the mobilised sediment was exported in the first year[21]. And yet, much lower yields are more typical, such as in the Matiri River (New Zealand), where at least 50–75% of the sediment generated by the 1929 Murchison Earthquake remained in the catchment 50 years later[13]. Evacuation of the 1999 Chi-Chi Earthquake debris filling the Peikang River is predicted to take centuries[18,22], just as 70% still remains intact of the 5–7 km^3 of sediment injected into the Pokhara Valley (Nepal) by medieval earthquakes[23].

In line with sediment flux, OC export from seismically active mountain belts varies widely: 0.12–0.28 teragrams (Tg C) per year following the Gorkha Earthquake[24] and up to 35–40 Tg C per year to the offshore of Taiwan[25], while a sediment record from Lake Paringa indicates that 14 ± 5 Tg C was eroded during a single earthquake on New Zealand's Alpine Fault[3]. Nevertheless, existing research on post-earthquake carbon dynamics has tended to focus on sediment fluxes and revegetation[26,27], whereas the role of transient OC storage held within landslides has been overlooked. We propose that the observed worldwide variation in carbon export reflects either (1) differences in the primary mass of OC mobilised during an earthquake, or (2) the potential for landslides to function as transient stores (a "capacitor effect") that mediate the release of sediment and OC beyond the mountain belt. These two hypotheses serve as the focus for our study.

The 2008 M_w7.9 Wenchuan Earthquake is a large historical landslide event of between 3 and 15 km^3 (6000–30,000 Tg of sediment, assuming an average density of landslide deposits of 2000 kg/m^3) of erosion[19]. Thanks to the intensive study of the resultant sediment cascade[19], Wenchuan is one of the best understood examples of post-earthquake erosional response. The earthquake struck at a time of rapid expansion of satellite technologies, which have allowed researchers to constrain the frequency and intensity of landsliding, the reworking of sediment from landslides into the drainage network, and the changes in vegetation coverage after the event[28,29]. As the largest earthquake-triggered landsliding event of the past 50 years, the Wenchuan example provides a unique opportunity to understand the carbon dynamics at scale. Our analysis therefore aims to constrain the potential upper bound of landslide-driven carbon storage and transient carbon transfer in mountain systems, rather than to represent the average behaviour across all earthquakes. Well-established river gauging in the affected region revealed a doubling of particulate OC transport via streams in the Zagunao catchment in the first four years[4], but the post-earthquake analysis remains incomplete. Here, we present a comprehensive OC budget for the period, 2008–2020, by integrating fieldwork, laboratory analyses, remote sensing and numerical modelling. Mapping of carbon stocks pre- and post-earthquake allows us to quantify the hillslope carbon mass balance for this earthquake with unprecedented precision. This framework further enables us to assess the long-term trajectory of carbon storage within mountainous landscapes.

Results

Spatial distribution of carbon and its erosion by landslides

We set out to identify and measure carbon stocks directly in the field at 123 sites comprising landslide deposits and areas undisturbed by earthquakes across the Longmenshan study area (Fig. 1). These field data are augmented with data extracted from previous studies. A subset of our dataset, scored for high quality, was incorporated into a machine-learning model that aims to simulate retrodictively the spatial distribution of carbon stocks prior to the Wenchuan Earthquake (Fig. 1A) based on a wide range of parameters (Table S1) (see Methods).

Prior to the Wenchuan Earthquake, we estimate the average OC stock across the Longmenshan study area (Fig. 1) at 136 ± 25 megagrams carbon per hectare (Mg C ha^{-1}), an average that embraces local variability of 50–260 Mg C ha^{-1} (note that all uncertainties are given as ±1 standard deviation, unless otherwise stated; units for carbon stock are presented as Mg C ha^{-1} and carbon flux is expressed as Mg C km^2 yr^{-1}). The spatial distribution of pre-earthquake OC stock correlates with topography and climate. The OC (within surface soil and vegetation) increases with elevation between 500–2000 metres above sea level (masl) but varies little outside that range (Figs. S1, S2). The highest concentration of total OC is found on the steepest mountains close to the range front where average precipitation rates are also highest (Fig. 1A, B).

Wenchuan landslides eroded 5.5 ± 0.01 Tg C, amounting to 2–6 weight percent (wt%) of global annual terrestrial carbon erosion[30]. The spatial distribution of landsliding relates to topography, lithology, and position relative to the fault rupture[31,32], and the majority (2.5 ± 0.6 km^3) of the landslide volume occurred within the Minjiang and Tuojiang basins (Fig. 1B). Corresponding erosion of OC by landslides in these two catchments equalled 4.5 ± 0.01 Tg C, which accounts for 82 ± 0.2% of the overall OC denuded by landslides associated with this event. The large OC stock in the Fujiang catchment remained largely intact, consistent with the spatial distribution of pre- and post-earthquake net primary production (NPP), which saw little change over this area (Fig. S3). These eroded OC are rapidly mobilised and widely deposited along hillslopes and channels, awaiting further transport or transformation.

Recovery of carbon stocks following landslides

A decade after the Wenchuan Earthquake, landslides stored 33 ± 21 Mg C ha^{-1} of OC in the study area (Fig. 2B). The recovery rate (i.e., growth) of OC was 475 ± 110 Mg C km^{-2} yr^{-1} on landslide surfaces and 5.5 ± 0.02 Mg C km^{-2} yr^{-1} when applied to the overall affected area, reflecting that landslides account for only about 8% of the total landscape area. The major components of the OC storage at these sites were soil OC (55 ± 29%) and tree biomass (32 ± 29%) (Fig. S4). Soil OC content is positively correlated with total soil nitrogen content (TN) for all sites (Fig. S5). New vegetation on landslide surfaces (including both deposit and scar areas) accounts for a quarter of the pre-earthquake OC stock (Fig. S6). Recovery was characterised by a major change in the species composition from a pre-earthquake community of *Pinus tabuliformis*, *Cupressus funerbris* and *Cryptomeria fortunei* to a recovery community of *Alnus cremastogyne*, *Populus alba* and *Ziziphus jujuba* (Fig. S7).

Vegetation coverage on landslide surfaces had recovered to 80–90% of pre-earthquake levels within a decade, as inferred from metrics including normalised difference vegetation index, enhanced vegetation index, leaf area index[28,33,34]. This observation is consistent with time series of net primary productivity (NPP) changes in our study area (Fig. 2B). Here, NPP was used solely to assess the temporal recovery of vegetation productivity, not as a direct measure of total carbon storage. NPP of both the whole landscape and landslide areas decreased immediately after the earthquake from 760 ± 110 Mg C km^{-2} yr^{-1} (in 2007) to a low point of 580 ± 120 Mg C km^{-2} yr^{-1} (in 2010), after which NPP recovered rapidly and reached pre-earthquake levels around 2015. Despite the rapid increase in NPP during this initial stage of recovery, total carbon storage within the landscape remained deficient due to the slower return of soil carbon and vegetation biomass (Fig. 2). Landslide surfaces sequestered 3.5 ± 0.01 Tg C via NPP, referring to the amount of OC fixed by plant photosynthesis minus losses from plant respiration. The upscaled OC, derived from field-measured OC, for landslide surfaces is 2.2 ± 0.01 Tg C, which is much smaller than the pre-earthquake level of 5.5 ± 0.01 Tg C. The field-measured OC represents the combined carbon storage in soil and vegetation biomass. The measured OC was about 10% lower than the NPP-derived estimate, which could partly reflect measurement uncertainty[35], in addition to potential carbon loss via fluvial transport, decomposition, and soil respiration.

https://doi.org/10.1038/s41467-026-68341-3

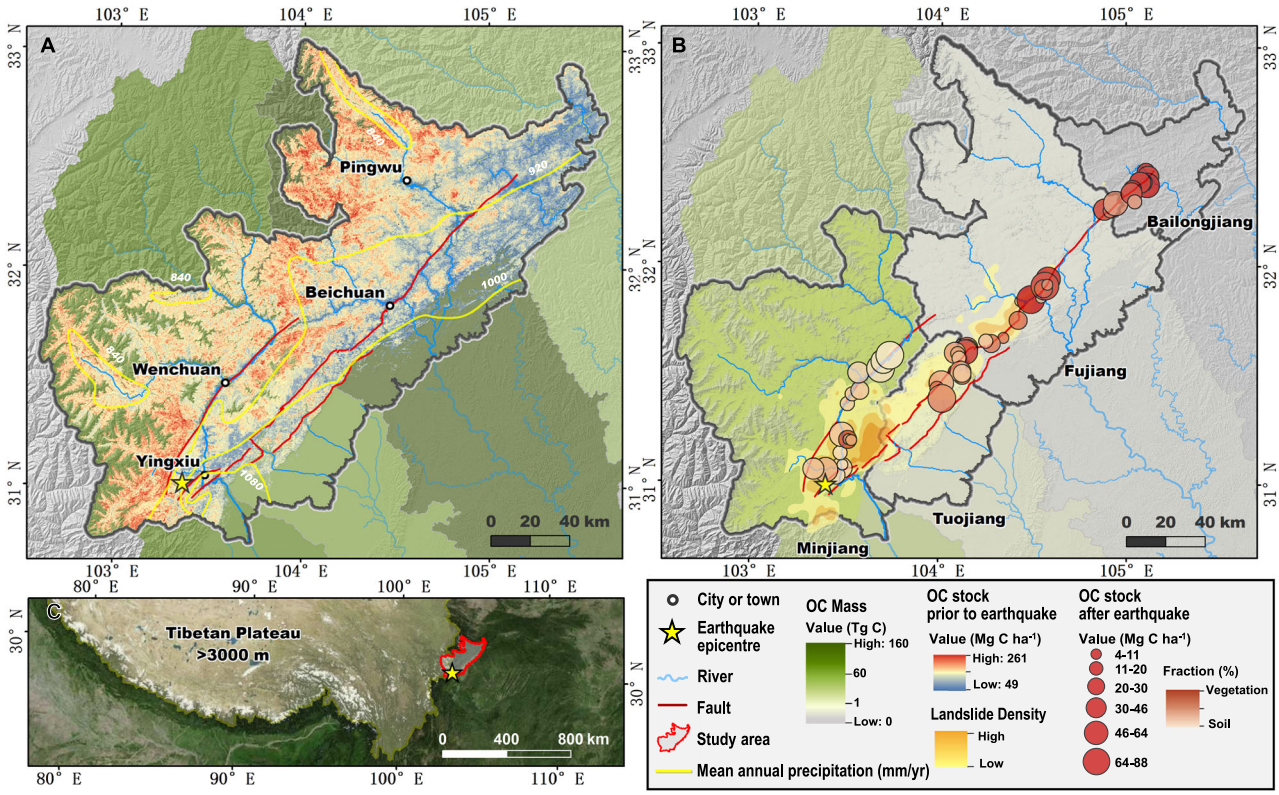

Fig. 1 | Spatial distribution of total organic carbon (OC) across the Longmenshan Range. A OC stock undisturbed by landslides (representing the OC stock prior to earthquake). **B** OC stock recovered after earthquake; grey boundaries mark the four major river catchments: Minjiang, Tuojiang, Fujiang and Bailongjiang. **C** Study area location at the southeastern margin of the Tibetan Plateau delineated by elevations >3000 m above sea level (masl). In (**A**) and (**B**), the semi-transparent backgrounds shows OC mass values, with (**A**) showing mass mobilised by coseismic landslides and (**B**) showing mass recovered after earthquake until 2020. Disc size is scaled to total OC stock on sampled landslide deposits (in Mg C ha^{-1}) after 10 years, and disc shading represents the relative fractions of vegetation OC and soil OC, as indicated by the colour scale shown in the figure. Map data: Google, Maxar Technologies, Esri.

Hillslope carbon budget after an earthquake

Using our estimates of burial and recovery of OC after the Wenchuan Earthquake, we calculated the hillslope carbon budget for the decade after the earthquake (Table S2). We determined the total volume of carbon stored in landslides (Fig. 3) based on the sediment export flux to the fluvial system from prior work[12], together with our results showing that pre-earthquake soil and vegetation OC are well mixed in landslide deposits—allowing us to assume that the proportional removal of OC is similar to that of sediment. On this basis, we estimate that 12% of the carbon stored in landslide deposits has been evacuated, primarily by debris flows[12]. The OC yield implied in this calculation falls within the uncertainty range of field measurements from the Zagunao catchment in the study area[4,36]. As an upper bound for erosion, we can also assume that all of the material in landslide deposits that are connected to the fluvial network has been evacuated, resulting in the removal of 43% of carbon mobilised by landslides[20]. Considering this range, hillslope landslide deposits apparently retained between 3.1 and 4.8 Tg C of the mass that was previously held in soils and vegetation. Based on field observations and the detailed sediment budget for this event[12], storage is likely to be closer to the upper bound of 4.8 Tg C. Meanwhile, 2.2 ± 0.01 Tg C was restored on the hillslopes. Overall, the Wenchuan Earthquake has stored up to 7.0 Tg C within landslide-affected areas between 2008 and 2020 (Fig. 3).

Discussion

The OC stock prior to the 2008 Wenchuan Earthquake is shown to be spatially correlated with landslide activity concentrated along the range front following the event. On the one hand, this spatial coincidence of high OC and landsliding could be spurious: the range front receives relatively high precipitation that enhances biological productivity and promotes the conversion of litter into soil OC. Moreover, mid- to high-elevations exhibit high terrestrial OC (Fig. S1) and lower temperatures can facilitate OC preservation in high-elevation soils by inhibiting respiration. Steep slopes at these elevations also drive more frequent landsliding. On the other hand, the observed correlation is consistent with feedback between soil carbon accumulation and landslide susceptibility. Vegetation and soil developed in landslide-prone terrain are frequently disturbed and buried. Prior work suggests that this kind of disturbance may foster soil OC assimilation and preservation, in part because biomass and soil carbon (reworked by landslides) can increase soil fertility, favouring the physical and microbial stabilisation of OC[37–39]. In field experiments, plants and soil buried by landslides increased organic matter accumulation more rapidly than natural plant litter[40]. In other studies, young landslide scars have been shown to store more OC in soils than in plant biomass, indicating the important role of landslides in storing soil OC[37].

In this study, the restored OC mainly derives from soil OC accumulation and preservation[27]. Catchments subject to the highest proportion of landslides (Minjiang and Tuojiang) also comprise the highest soil OC stock, accounting for 59% to 87% of overall OC. The enhanced soil OC in the Minjiang and Tuojiang areas suggests either that landslide disturbances have promoted soil carbon accumulation, or some fraction of buried woody debris and soil OC was inherited pre-2008. This inheritance effect cannot simply be due to direct transfer and immediate deposition of soil OC. In fact, where the OC content of landslide deposits has been measured in other studies, it is close to zero: reported values include 0.17 ± 0.04% for the top 10 cm in a tropical forest in Puerto Rico[41]; 0.15 ± 0.05% for rockslides in the western

https://doi.org/10.1038/s41467-026-68341-3

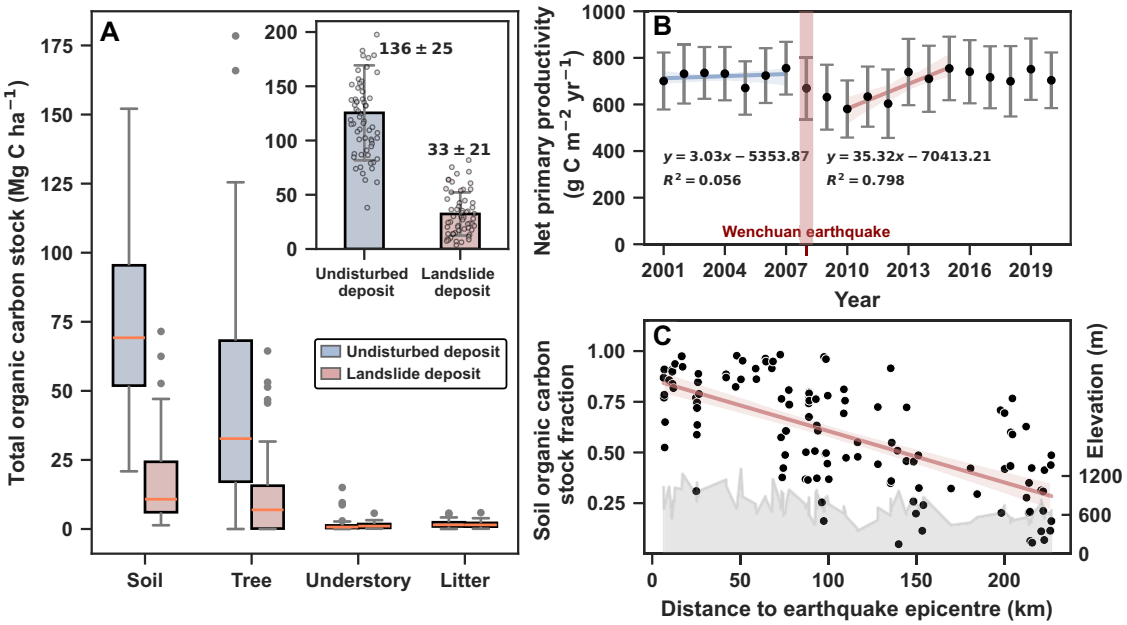

Fig. 2 | Composition of organic carbon (OC) stock in the landslide-affected areas. A Soil OC, tree OC, understorey plant OC and litter OC on undisturbed deposits (UD) that represent conditions prior to earthquake, and landslide deposits (LD) representing the conditions after earthquake as measured in the field. The inset shows the total OC stocks. Box-and-whisker plots display the data distribution, where central line indicates the median, box limits represent the upper and lower quartiles, whiskers extend to 1.5 times the interquartile range, grey dots denote outliers, and error bars represent one standard deviation. **B** Annual trend in net primary productivity (NPP) on undisturbed and landslide deposits. **C** Fraction of Soil OC relative to total OC stock as a function of the distance to the Wenchuan Earthquake epicentre.

Southern Alps[8]. The initial content of fresh deposits is less than ~10% of the current content. Such inheritance may occur because the disturbed soil OC and carbon-rich debris might be diluted or deeply buried, and gradually converted to soil OC via soil formation processes. The typical carbon sink of forests in southwest China ranges between 66 and 122 Mg C km^{-2} yr^{-1}[42,43]. Although the soil OC accumulation rate after landsliding is expected to be higher compared to undisturbed soils, the rate of soil OC accumulation on landslide scars in Taiwan—where overall OC is much higher than that in Southwest China—was approximately 200 Mg C km^{-2} yr^{-1} following initial revegetation. For Wenchuan sites, soil OC accumulation rates range between 12 and 596 Mg C km^{-2} yr^{-1}. The upper bound significantly exceeds both the natural carbon sink in the study area and values reported in other regions, suggesting the additional legacy carbon sources may have contributed to rapid soil OC production.

The 2008 Wenchuan Earthquake mobilised OC estimated at 5.5 ± 0.01 Tg, which is within the range reported for other landslide events (Table 1); for example, landslides associated with Alpine Fault (NZ) earthquakes and typhoons following the Chi-Chi Earthquake[17] generated between 3 and 14 Tg C. Nevertheless, the amount of mobilised carbon is influenced by the environmental setting of the study area and the baseline OC fluxes prior to disturbance. The Liwu River case study reports higher OC yield, mainly owing to its typhoon-induced landslides, high biomass production and maritime/tropical climate, which also drive higher rates of fluvial particulate OC and OC restoration. In these cases, the high intensity of mobilised or transported OC does not necessarily correspond to regions with high landslide density; instead, it may depend on additional factors such as primary productivity, sediment yield, and fluvial transport capacity[44,45]. By comparison, rates of OC accumulation after the Wenchuan Earthquake are higher than in many studies, perhaps due to the lower export rates of fluvial particulate OC for the Wenchuan event. In the Narayani basin (central Himalaya), following the 2015 Gorkha Earthquake, coseismic landslides did not significantly perturb sediment and carbon fluxes[24]. A possible explanation based on our study is that most of the sediment and OC generated by coseismic landslides were buried and not exported from the mountain belts in the short term[12,46]. Overall, our carbon budget highlights the governing role of landslides as a carbon store, with carbon export rate dependent on remobilisation via mass movement processes. However, estimates of mobilised sediment remain fundamentally constrained by landslide volume calculations derived from area-volume scaling relationships (Table S11 and S12). As a result, uncertainties associated with landslide volume estimation therefore likely represent one of the dominant sources of uncertainty in our results and in the referred carbon budget[47].

Our OC budget for the Wenchuan Earthquake demonstrates how the total OC stock (the sum of vegetation OC, soil OC and buried OC) may respond following large earthquakes (Fig. 4A). Prior to the Wenchuan event, the Longmenshan region contained a mature forest ecosystem that was approaching an equilibrium state. Immediately after the earthquake, living biomass and pre-existing soil OC were buried by landslides. The evacuation of OC from landslide deposits to the drainage network exceeded the sequestration of soil OC from litter and woody debris[48], resulting in a net decrease in soil OC stock (Fig. 4B). And yet, despite some erosion, approximately 88% of OC associated with landslides remained on the hillslopes a decade after the earthquake[12]. With vegetation regrowth on these deposits, the total OC shows an increasing trend, with peak values reaching ~4% of the pre-equilibrium state. With the landslide proportion ranging from 10 to 50%, the total OC fluctuates by ~10%. This storage capacity of OC in landslide deposits, which has not been widely considered in prior work on post-earthquake carbon dynamics, may play an important role in the evolution of OC storage. Nevertheless, over time the OC stored in landslide deposits will be released, either via in situ decomposition or via export of the material into the river system and out of the mountain belt.

Following the Wenchuan Earthquake, we predict that the terrestrial ecosystem will require approximately 170 ± 10 years, 110 ± 500 years and 1800 ± 500 years for vegetation OC, buried OC and soil OC, respectively, to return to their pre-earthquake equilibrium levels. The

https://doi.org/10.1038/s41467-026-68341-3

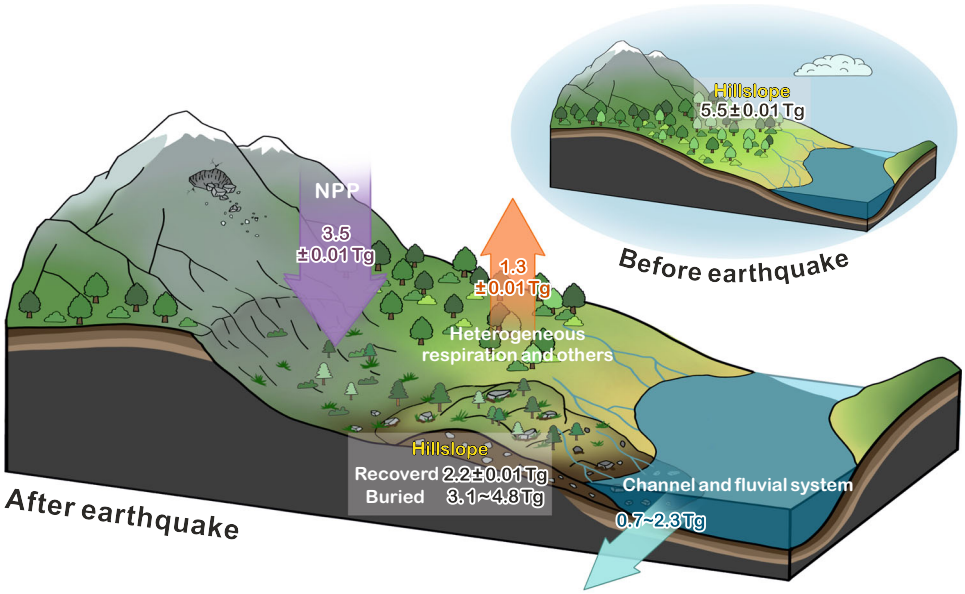

Fig. 3 | Overview of hillslope organic carbon (OC) budget triggered by the 2008 Wenchuan Earthquake. Arrows represent carbon fluxes, and grey boxes indicate hillslope carbon stocks within landslide-affected areas. Numbers denote the accumulated OC mass associated with these processes from the time of the 2008 Wenchuan Earthquake to 2020; values are reported as mean ± standard deviation (SD). Details of the carbon budget construction are provided in the Supplementary Information. Calculation of OC stocks prior to the earthquake and recovered OC stocks after the earthquake are presented in Table S3.

net effect of total OC, as illustrated in Fig. 4B, suggests that hillslopes act as an organic carbon capacitor, storing carbon in landslide deposits and slowly releasing it by respiration and erosion. The transition from a net carbon sink to a net carbon source reflects the balance between the asymptotic limit of vegetation regrowth and prolonged release of buried OC; the timescale required to reach equilibrium is governed by long-term mass movements that control OC transport from landslide deposits. This timescale is comparable to the return period of large earthquakes in the region[46]. The interval between earthquakes with a magnitude of >Mw 7.9 in the Longmenshan region is ~1800 years[49,50]. However, during this period, other earthquakes with magnitudes less than Mw 7.9 occur frequently, suggesting that the impact is not limited to a single earthquake event. These frequent earthquakes may result in cumulative effects on mountainous carbon storage, contributing to a net carbon sink over the long term.

Methods

Sampling sites

Our study area covers 33,005 km^2 of the region most severely affected by the 2008 M_w 7.9 Wenchuan Earthquake. Landslides occurred primarily in mountainous terrain within four large river systems: the Minjiang, Tuojiang, Fujiang and Bailongjiang (Fig. S8). We selected 123 sampling sites for field investigation, of which 59 were on coseismic landslide deposits (disturbed sites) and 64 were on adjacent undisturbed areas with no clear slope failure (since 2008) based on aerial and satellite imagery. The disturbed sites were randomly distributed along the major faults of the Longmenshan that ruptured during the earthquake.

Plot design

The plot design for sampling followed previous studies in the Luoquanwan catchment[51,52]. Measured OC is composed of soil, tree, understorey plant and litter OC. The simplified vegetation OC represents the tree, understorey plant and litter OC. Within a 5-m radius plot (after slope correction), all trees with a diameter at breast height (DBH) > 5 cm were recorded for species, DBH and total height (Table S2). Heights of trees were measured in each plot using a Vertex III height meter (Haglöf, Sweden). Plants with DBH < 5 cm were considered as understorey. To estimate biomass of the understorey and litter, three 1-m radius circular subplots were set at three directions (0°, 120°, 240°, 3 m from the plot centre) within the 5-m radius plots. Understorey and litter within each subplot were dried and weighed. Within the three subplots, soil samples were collected in cloth bags down to 50 cm in three layers: 0–10 cm, 10–30 cm, and 30–50 cm, respectively. Soil samples from the same layer were mixed for each given sub-plot location. Soil samples were collected using standard ring cores with a diameter of 70 cm for each layer to analyse soil physical properties in undisturbed areas. Due to the high gravel content of landslide deposits, a circular bucket with fixed volume was used to obtain the wet density for different layers. A detailed list of collected samples is shown in Table S4.

Landslide inventory

We used a published landslide inventory to calculate the total carbon budget[32]. This dataset covers over 90% of the surface rupture area and the zones of most concentrated landslide density. The approach for constructing the carbon budget is described in detail in the Supplementary Information. Estimates of carbon storage in coseismic landslides include only failures >5800 m^2, consistent with the 30×30 m resolution of the prediction model described in the method of modelling of carbon stock. Landslides >10,000 m^2 were selected for field sampling as they were easily recognized from satellite images. The mass of total OC, as determined through gridded data, is presented in Table S3 pre-earthquake, along with the mobilisation and recovery post-earthquake.

Landslide volume and area

To model the carbon balance following the 2008 Wenchuan Earthquake, it is essential to estimate landslide volumes, which directly determine the timescale of sediment and carbon transport. We used a common approach of applying a power-law volume-area relationship to convert the landslide inventory to landslide volumes. There is significant uncertainty with this approach[47], but the satellite imagery available to us precludes a more accurate volume-based approach. Instead, we use a range of different area-volume scaling parameters and scar-deposit correction methods, as detailed in Supplementary

Table 1 | Compilation of organic carbon (OC) data following major perturbations

Study Site	Study area (km^2) [a]	Disturbance (return period)	OC mobilised by landslides (Tg C) [b]	OC yield averaged by return period (Mg C km^{-2} yr^{-1}) [c]	Fluvial POC export (Mg C km^{-2} yr^{-1}) [d]	OC recovery rate (Mg C km^{-2} yr^{-1}) [e]	Cita-tion
Kotatahi valley, Southern Alps, New Zealand	2434	Landslides (~40 y)	0.7 ± 0.3	7.6 ± 2.9	39	94 ± 11	6,8
Windbag basin, Southern Alps, New Zealand	60	Coseismic landslides (250–350 y)	8.0 ± 4.0 to 14.0 ± 5.0	5 ± 2 to 9 ± 4	NA	NA	3,8,62
Sierra de Las Minas Mts, Guatamala	657	Hurricane (20–80 y)	0.4×10^6	8–33	NA	4.42–22.12	7
Zagunao River, Longmenshan, China	4629	Coseismic landslides	0.2 ± 0.0	1.23	1.23 ± 0.57	NA	4,36
Longmenshan, China	33005	Coseismic landslides (~80 y)	5.5 ± 0.01	2.1 ± 0.004	1.45 ± 0.1	5.5 ± 0.02 (475 ± 110)	This study
LiWu River, Taiwan	3320	Typhoons (~50 y)	3.9 ± 0.6	23.7 ± 3.9	16-202	~200 (282–445)	44,45
Alsea River, Oregon Coast Range, USA	865	Landslides	NA	NA	3.8	NA	63
Redwood Ck, California Coast Range, USA	718	Storm-triggered landslides (10 y)	0.02	2.8	NA	NA	64
Kosñipata Valley, Andean Plateau, Peru	143	Storm-triggered landslides (25 y)	0.1 ± 0.0	26 ± 4	NA	225–326	65,66

This covers landslides–mobilised OC, fluvial particulate OC, and overall OC recovery rate associated with coseismic landslides.

[a]Study area is considered a drainage area for catchment-based studies, or an administrative division in a disturbance-affected region.

[b]OC mass mobilised by landslides is calculated as landslide area multiplied by total OC stock (per unit area) prior to or without the disturbance of landslides.

[c]OC yield is the total OC mass mobilised, averaged by area and corresponding return period of disturbance.

[d]Fluvial POC export calculated from POC content and suspended sediment discharge. Total flux may include petrogenic POC and ecosystem POC. The POC export in the LiWu river is estimated by the suspended sediments collected at Lushui gauging station, LiWu river, from 1970.

[e]OC recovery rate is the total OC restored after disturbance over a specific period, which can be directly sampled by forest plots or indirectly characterized by net ecosystem production (NEP, practically NPP reduces soil heterotrophic respiration and decomposition) or other indices. Values in parentheses are the total recovered carbon amount applied to the denuded landslide area only.

https://doi.org/10.1038/s41467-026-68341-3

https://doi.org/10.1038/s41467-026-68341-3

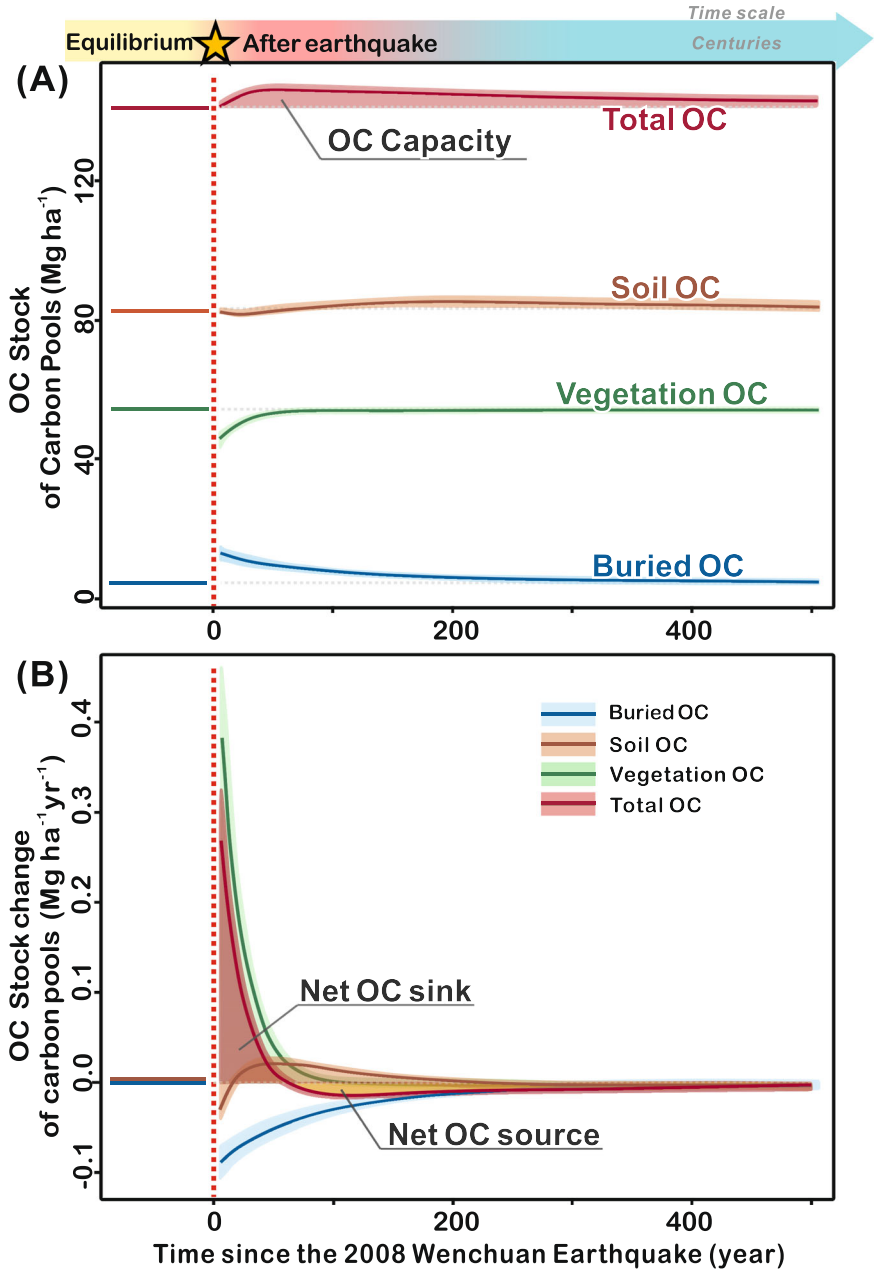

Fig. 4 | Evolution of carbon stocks for major hillslope carbon pools following the 2008 Wenchuan Earthquake. A ecosystem organic carbon (OC) stock over time. The red-shaded zone represents the OC capacity of storage after earthquake. **B** OC stock change over time. The red-shaded zone marks the period when the hillslopes function as a net OC sink, and the yellow-shaded zone marks the period when hillslopes function as a net OC source. The major carbon pools in this study include soil carbon pool (Soil OC), vegetation carbon pool (Vegetation OC) and buried carbon pool (Buried OC). The Total OC is the sum of these carbon pools. The buried OC represents the destroyed vegetation and soil OC by landslides and buried under landslides deposits.

Information. None of the available landslide inventories distinguishes between landslide types or between source and deposit areas making direct inferences about volume a challenge. Here we have compared different approaches to estimate the potential range of volume uncertainty (Tables S11S12).

Soil physical properties, organic carbon and total nitrogen

All soil samples were dried in an oven at 85°C to a constant weight. Bulk density, water content, and gravel fraction (>2 mm) were analysed following standard methods[53]. For the disturbed sites, wet density was measured in the field. Identifiable plant residues and roots were removed manually, and samples were sieved at 0.15, 0.25, 0.5, 1.0, 2.0, and 5.0mm intervals. Soil OC content was analysed using the potassium dichromate and sulphuric acid ($K_2Cr_2O_7$–H_2SO_4) wet oxidation method[54]. Total nitrogen (TN) content was determined by the automatic Kjeldahl apparatus method following the Chinese Agriculture Industry Standard (NY/T 1121.24-2012). Both soil OC and TN analyses were repeated three times for each sample.

Vegetation biomass calculation

Tree biomass was calculated using a dataset of Chinese allometric equations[55]. We estimated above-ground and below-ground biomass by selecting the appropriate allometric relationship based on the tree species, diameter and height range, mean annual precipitation (MAP), mean annual temperature (MAT), and location. For species not found in the database, we applied the general allometry by plant functional

group (e.g., deciduous broad-leaved forest or evergreen broad-leaved forest). We included all major biomass components, including stem, branch, leaf, and below-ground biomass. Tree species and related allometric models are given in Table S5. All sampled understorey vegetation and litter samples within three 1-m radius circular subplot were dried at 70°C to a constant weight. Carbon content of 0.5 g•g^{-1} was used to convert biomass to C stock[54].

Soil OC stock

The soil organic C stock (Mg ha^{-1}) for each layer was calculated using the following formula[56]:

$$SOC_{stock} = SOC \times BD \times (1 - RC) \times D/10$$

where total SOC stock (Mg C ha^{-1}) is the soil OC concentration (g•kg^{-1}); *BD* is bulk density (g•cm^{-3}); *RC* is gravel (>2 mm) content; *D* is soil layer depth (cm).

Data compiled from previous studies

We compiled previously published OC data from the study area (194 entries derived from 25 publications), focusing on studies that report field sampling data in undisturbed forest and shrub ecosystems, excluding those based on models or satellite data, as well as planted forests. For inclusion data must include geographical coordinates, and at least one of the following: soil organic carbon, above-ground and below-ground biomass, or total carbon (see Fig. S9). Data quality was evaluated by assigning scores, 0–2, based on eight categories (namely data type, data information, climate information, geographic information, soil information, soil organic carbon, vegetation organic carbon and total terrestrial organic carbon), with the maximum cumulative score being 16 (see Table S6). This dataset will serve as a reference for further research conducted in the Longmenshan Range or the Tibetan Plateau (see Source Data 1).

For the training of the machine-learning predictive model, we utilized previous study datasets scoring >5, together with our own field-measured dataset. Soil C stock was normalised to a depth of 50 cm; for soil profiles <50 cm, extrapolation was performed by averaging the C content and dry bulk density from known depths and then applying it to 50 cm. The augmented data helps to overcome the spatial limitations inherent in our field-measured dataset.

Modelling of carbon stock

During preliminary screening, we trialled twenty different predictive models to identify the most suitable for total OC stock; these included: random forest, gradient boosting decision trees (GBDT), extreme gradient boost, decision tree, support vector regression, k-nearest neighbour regression, linear weight regression, etc. Twenty covariates derived from remote sensing data, geographic data and landslide inventory were applied[57–59]. The prediction models were built using representative topographic and soil characteristics, climatic, and vegetation indices across the study area, and include landslide area, slope, aspect, elevation, lithology, MAP, MAT, land surface temperature, TN, clay content, bulk density, Landsat derived enhanced vegetation index, normalised difference vegetation index, red band and modified soil adjusted vegetation index, MODIS product (MOD17A3) derived enhance vegetation index, normalized difference vegetation, red band and modified soil adjusted vegetation index and gross primary production, as specified in Table S1. The raster maps of these variables were resampled to 10 m resolution for spatial calculation, consistent with DEM resolution.

To ensure that our model was applied only to forest ecosystems, we used the 30 m Landsat-derived annual land-cover dataset for China[60] to define land use types (with categories: forest, shrub, grassland, wetland, farmland, urban and other), and areas not identified as forest or shrub were excluded.

We trained the machine-learning prediction model using the total carbon stock data from our field-measured data and the twenty covariates noted above. We developed models for disturbed and undisturbed sites trained using 70% of the field sampling data, leaving the remaining 30% for testing. After training and testing, we found that the GBDT method was the best performer (see Table S7). Figure S10 presents the importance of covariates within the training samples as identified by the GBDT.

Modelling of carbon balance

To quantify the temporal trend of major carbon pools under the impact of the 2008 Wenchuan Earthquake, our carbon balance model adopts a pool–flux structure[61], employing a set of differential equations to simplify the connection between carbon flux and mass movements. We derived the parameters for the carbon balance model by integrating subsequent research and data collected since the Wenchuan event (particularly the carbon stock distribution maps obtained from empirical data noted above). This approach ensures that the parameter settings are tailored to our study area and effectively reflect complex environmental interactions. The carbon balance modelling separates into three main parts: constructing the carbon balance framework, introducing earthquake-triggered landslides and implementing carbon balance model. The model is based on two key assumptions: (1) following the earthquake, the entire aboveground biomass carbon pool (B) is converted into debris (D) that is fully mixed with soil carbon and buried within landslide deposits. Because this exact initial B–D portioning lacks empirical constraint, it represents a source of uncertainty in the estimated long-term carbon storage. This assumption represents an endmember maximum potential carbon storage after the earthquake; (2) ecosystems outside the landslide surface areas are assumed to have remained undisturbed, regions showing no bare surfaces or vegetation loss are assumed to have the same stock before and after the earthquake. The major carbon pools and fluxes are shown in Fig. S11.

Statistical analyses

For our field data, descriptive statistical analyses were conducted to characterise the spatial variations of soil organic carbon (SOC) content, soil total nitrogen (TN) content, and soil OC stock with depth, as well as tree, understory, litter, and total ecosystem organic carbon stocks in both undisturbed areas and landslide deposits (Table S8). Prior to model training, multicollinearity among covariates was evaluated using Pearson correlation analysis (Fig. S12). For the modelling of carbon stock analysis, we applied the Shapiro–Wilk test to examine the representativeness and normality of twenty selected covariates (see Table S9). Subsequently, a one-way analysis of variance (ANOVA, F test) was used to test whether the effect of coseismic landslides on OC stock is distinguishable ($p < 0.05$) when comparing undisturbed areas and landslide deposits (see Table S10).

Data availability

The data generated or analysed during this study are included in the paper, Supplementary Information and the Source Data 1. Source data are provided with this paper.

Code availability

The codes to produce the carbon balance model are available at https://github.com/liujie1408/carbon-dynamics-model

References

1. Chen, H., Wu, N., Yuan, X., Gao, Y. & Zhu, D. Aftermath of the Wenchuan earthquake. *Front. Ecol. Environ.* **7**, 72 (2009).
2. Stone, R. Wenchuan earthquke—a deeply scarred land. *Science* **324**, 713–714 (2009).

3. Frith, N. V. et al. Carbon export from mountain forests enhanced by earthquake-triggered landslides over millennia. *Nat. Geosci.* **11**, 772–776 (2018).
4. Wang, J. et al. Earthquake-triggered increase in biospheric carbon export from a mountain belt. *Geology* **44**, 471–474 (2016).
5. Carey, A. E., Gardner, C. B., Goldsmith, S. T., Lyons, W. B. & Hicks, D. M. Organic carbon yields from small, mountainous rivers, New Zealand. *Geophys. Res. Lett.* **32**, L15404 (2005).
6. Hilton, R. G., Meunier, P., Hovius, N., Bellingham, P. J. & Galy, A. Landslide impact on organic carbon cycling in a temperate montane forest. *Earth Surf. Process. Landf.* **36**, 1670–1679 (2011).
7. Ramos Scharrón, C. E., Castellanos, E. J. & Restrepo, C. The transfer of modern organic carbon by landslide activity in tropical montane ecosystems. *J. Geophys. Res.: Biogeosci.* **117**, 2553 (2012).
8. Hilton, R. G., Galy, A. & Hovius, N. Riverine particulate organic carbon from an active mountain belt: Importance of landslides. *Global Biogeochem. Cycles* **22**, 1–12 (2008).
9. Kao, S.-J. & Liu, K.-K. Particulate organic carbon export from a subtropical mountainous river (Lanyang Hsi) in Taiwan. *Limnol. Oceanogr.* **41**, 1749–1757 (1996).
10. Hovius, N. et al. Prolonged seismically induced erosion and the mass balance of a large earthquake. *Earth Planet. Sci. Lett.* **304**, 347–355 (2011).
11. Hunter, B. D., Roering, J. J., Silva, L. C. R. & Moreland, K. C. Geomorphic controls on the abundance and persistence of soil organic carbon pools in erosional landscapes. *Nat. Geosci.* **17**, 151–157 (2024).
12. Francis, O. et al. The Fate of Sediment After a Large Earthquake. *J. Geophys. Res.: Earth Surf.* **127** (2022). https://doi.org/10.1029/2021jf006352
13. Pearce, A. J. & Watson, A. J. Effects of earthquake-induced landslides on sediment budget and transport over a 50-yr period. *Geology* **14**, 52–55 (1986).
14. Korup, O. Earth's portfolio of extreme sediment transport events. *Earth-Sci. Rev.* **112**, 115–125 (2012).
15. Korup, O. Geomorphic imprint of landslides on alpine river systems, southwest New Zealand. *Earth Surf. Process. Landf.* **30**, 783–800 (2005).
16. Koi, T. et al. Prolonged impact of earthquake-induced landslides on sediment yield in a mountain watershed: The Tanzawa region, Japan. *Geomorphology* **101**, 692–702 (2008).
17. Dadson, S. J. et al. Earthquake-triggered increase in sediment delivery from an active mountain belt. *Geology* **32**, 733–736 (2004).
18. Yanites, B. J. et al. The influence of sediment cover variability on long-term river incision rates: an example from the Peikang River, central Taiwan. *J. Geophys. Res. Atmos.* **116** https://doi.org/10.1029/2010JF001933 (2011).
19. Fan, X. et al. Earthquake-induced chains of geologic hazards: patterns, mechanisms, and impacts. *Rev. Geophys.* https://doi.org/10.1029/2018RG000626 (2019).
20. Li, G. et al. Connectivity of earthquake-triggered landslides with the fluvial network: Implications for landslide sediment transport after the 2008 Wenchuan earthquake. *J. Geophys. Res.: Earth Surf.* **121**, 703–724 (2016).
21. Pain, C. F. & Bowlersw, J. M. Denudation following the November 1970 earthquake at Madang, Papua New Guinea. *Z. Geomorphologie, N. F.* **18**, 92–104 (1973).
22. Yanites, B. J., Tucker, G. E., Mueller, K. J. & Chen, Y.-G. How rivers react to large earthquakes: Evidence from central Taiwan. *Geology* **38**, 639–642 (2010).
23. Stolle, A. et al. Protracted river response to medieval earthquakes. *Earth Surf. Process. Landf.* **44**, 331–341 (2019).
24. Märki, L. et al. An unshakable carbon budget for the Himalaya. *Nat. Geosci.* **14**, 745–750 (2021).
25. Hilton, R. G. et al. Climatic and geomorphic controls on the erosion of terrestrial biomass from subtropical mountain forest. *Global Biogeochem. Cycles* **26** https://doi.org/10.1029/2012GB004314 (2012).
26. Freund, C. A., Clark, K. E., Curran, J. F., Asner, G. P. & Silman, M. R. Landslide age, elevation and residual vegetation determine tropical montane forest canopy recovery and biomass accumulation after landslide disturbances in the Peruvian Andes. *J. Ecol.* **109**, 3555–3571 (2021).
27. Rasigraf, O. & Wagner, D. Landslides: An emerging model for ecosystem and soil chronosequence research. *Earth-Sci. Rev.* **231** https://doi.org/10.1016/j.earscirev.2022.104064 (2022).
28. Yunus, A. P. et al. Decadal vegetation succession from MODIS reveals the spatio-temporal evolution of post-seismic landsliding after the 2008 Wenchuan earthquake. *Remote Sensing Environ.* **236** https://doi.org/10.1016/j.rse.2019.111476 (2020).
29. Chou, W. C., Lin, W. T. & Lin, C. Y. Vegetation recovery patterns assessment at landslides caused by catastrophic earthquake: a case study in central Taiwan. *Environ. Monit. Assess.* **152**, 245–257 (2009).
30. Lal, R. Soil erosion and the global carbon budget. *Environ. Int.* **29**, 437–450 (2003).
31. Gorum, T. et al. Distribution pattern of earthquake-induced landslides triggered by the 12 May 2008 Wenchuan earthquake. *Geomorphology* **133**, 152–167 (2011).
32. Li, G. et al. Seismic mountain building: Landslides associated with the 2008 Wenchuan earthquake in the context of a generalized model for earthquake volume balance. *Geochem. Geophysics. Geosyst.* **15**, 833–844 (2014).
33. Wang, X. et al. Long-term landslide evolution and restoration after the Wenchuan earthquake revealed by time-series remote sensing images. *Geophys. Res. Lett.* **51**, e2023GL106422 (2024).
34. Sun, X. -f et al. Spatiotemporal change of vegetation coverage recovery and its driving factors in the Wenchuan earthquake-hit areas. *J. Mt. Sci.* **18**, 2854–2869 (2021).
35. Turner, D. P. et al. Site-level evaluation of satellite-based global terrestrial gross primary production and net primary production monitoring. *Glob. Change Biol.* **11**, 666–684 (2005).
36. Wang, J. et al. Controls on fluvial evacuation of sediment from earthquake-triggered landslides. *Geology* **43**, 115–118 (2015).
37. Walker, L. R. & Shiels, A. B. Post-disturbance erosion impacts carbon fluxes and plant succession on recent tropical landslides. *Plant Soil* **313**, 205–216 (2008).
38. Rammig, A., Fahse, L., Bugmann, H. & Bebi, P. Forest regeneration after disturbance: a modelling study for the Swiss Alps. *For. Ecol. Manag.* **222**, 123–136 (2006).
39. Velázquez, E. & Gómez-Sal, A. Environmental control of early succession on a large landslide in a tropical dry ecosystem (Casita Volcano, Nicaragua). *Biotropica* **39**, 601–609 (2007).
40. Shiels, A. B., Walker, L. R. & Thompson, D. B. Organic matter inputs create variable resource patches on Puerto Rican landslides. *Plant Ecol.* **184**, 223–236 (2005).
41. Guariguata, M. R. Landslide disturbance and forest regeneration in the upper Luquillo Mountains of Puerto Rico. *J. Ecol.* **78**, 814–832 (1990).
42. Pan, Y. et al. A large and persistent carbon sink in the world's forests. *Science* **333**, 988–993 (2011).
43. Guo, Z., Hu, H., Li, P., Li, N. & Fang, J. Spatio-temporal changes in biomass carbon sinks in China's forests from 1977 to 2008. *Sci. China Life Sci.* **56**, 661–671 (2013).
44. Hilton, R. G. et al. Tropical-cyclone-driven erosion of the terrestrial biosphere from mountains. *Nat. Geosci.* **1**, 759–762 (2008).
45. West, A. J. et al. Mobilization and transport of coarse woody debris to the oceans triggered by an extreme tropical storm. *Limnol. Oceanogr.* **56**, 77–85 (2011).

46. Francis, O. R. et al. The impact of earthquakes on orogen-scale exhumation. *Earth Surf. Dynam.* **8**, 579–593 (2020).
47. Jones, K. E. et al. An alternative to landslide volume-area scaling relationships: an ensemble approach adopting a difference model to estimate the total volume of landsliding triggered by the 2016 Kaikōura earthquake, New Zealand. *Landslides* **22**, 2219–2236 (2025).
48. Marc, O., Hovius, N., Meunier, P., Uchida, T. & Hayashi, S. Transient changes of landslide rates after earthquakes. *Geology* **43**, 883–886 (2015). %J Geology.
49. Gutenberg, B. & Richter, C. F. Magnitude and energy of earthquakes. *Ann. Geophys.* **53**, 7–12 (1956).
50. Li, G. et al. Earthquakes drive focused denudation along a tectonically active mountain front. *Earth Planet. Sci. Lett.* **472**, 253–265 (2017).
51. Liu, J. et al. Ecosystem carbon stock loss after a mega earthquake. *Catena* **216** https://doi.org/10.1016/j.catena.2022.106393 (2022).
52. Harvey, E. L., Hales, T. C., Hobley, D. E. J., Liu, J. & Fan, X. Measuring the grain-size distributions of mass movement deposits. *Earth Surf. Process. Landf.* **47**, 1599–1614 (2022).
53. Zhang, W., Yang, G., Tu, X. & Zhang, P. Determination of forest soil water-physical properties. *China Criterion of Forest Technique* (1999).
54. Fan, S. et al. Ecosystem Carbon Stock Loss after Land Use Change in Subtropical Forests in China. *Forests* **7** https://doi.org/10.3390/f7070142 (2016).
55. Luo, Y. et al. A review of biomass equations for China's tree species. *Earth Syst. Sci. Data* **12**, 21–40 (2020).
56. Xie, Z. et al. Soil organic carbon stocks in China and changes from 1980s to 2000s. *Global Change Biol.* **13**, 1989-2007 (2007).
57. Silatsa, F. B. T., Yemefack, M., Tabi, F. O., Heuvelink, G. B. M. & Leenaars, J. G. B. Assessing countrywide soil organic carbon stock using hybrid machine learning modelling and legacy soil data in Cameroon. *Geoderma* **367** https://doi.org/10.1016/j.geoderma.2020.114260 (2020).
58. Kunkel, V. R., Wells, T. & Hancock, G. R. Modelling soil organic carbon using vegetation indices across large catchments in eastern Australia. *Sci. Total Environ.* **817**, 152690 (2022).
59. Dai, L. et al. Influence of soil properties, topography, and land cover on soil organic carbon and total nitrogen concentration: A case study in Qinghai-Tibet plateau based on random forest regression and structural equation modeling. *Sci. Total Environ.* **821**, 153440 (2022).
60. Yang, J. & Huang, X. The 30 m annual land cover dataset and its dynamics in China from 1990 to 2019. *Earth Syst. Sci. Data* **13**, 3907–3925 (2021).
61. Booth, A. M., Buma, B. & Nagorski, S. Effects of landslides on terrestrial carbon stocks with a coupled geomorphic-biologic model: Southeast Alaska, United States. *J. Geophys. Res.: Biogeosci.* **128**, e2022JG007297 (2023).
62. Hilton, R. G. Climate regulates the erosional carbon export from the terrestrial biosphere. *Geomorphology* **277**, 118–132 (2017).
63. Hatten, J. A., Goñi, M. A. & Wheatcroft, R. A. Chemical characteristics of particulate organic matter from a small, mountainous river system in the Oregon Coast Range, USA. *Biogeochemistry* **107**, 43–66 (2010).
64. Madej, M. A. Redwoods, restoration, and implications for carbon budgets. *Geomorphology* **116**, 264–273 (2010).
65. Clark, K. E. et al. Storm-triggered landslides in the Peruvian Andes and implications for topography, carbon cycles, and biodiversity. *Earth Surf. Dyn.* **4**, 47–70 (2016).
66. Clark, K. E. et al. Erosion of organic carbon from the Andes and its effects on ecosystem carbon dioxide balance. *J. Geophys. Res.: Biogeosci.* **122**, 449–469 (2017).

Acknowledgements

The authors thank Prof. Zhangdong Jin for his constructive comments and valuable suggestions, which helped to improve this manuscript. We also thank Liyang Jiang, Shikang Liu, Yinshuang Yang and Tao Wei for their invaluable assistance with field sampling and laboratory experiments, Chengyong Fang for support with model computations, and Hao Zhong for helpful discussions on the mathematical treatment of uncertainty in landslide volume and sediment budget calculations. We further thank the reviewers for their constructive comments, which greatly improved the quality of this manuscript. This research was supported by the National Science Fund for Distinguished Young Scholars of China (Grant No. 42125702; X.F.), the National Natural Science Foundation of China (Grant No. 42507288; J.L.), the National Science Fund for International Cooperation and Exchange of China (Grant No. W2412050; X.F.), Key Program of Tianfu Yongxing Laboratory (Grant 2023KJGG06; X.T.), and the 111 Project.

Author contributions

Conceptualization: X.F., T.C., J.L. Methodology: J.L., X.T. Investigation: J.L., E.L.H. Visualization: J.L. Supervision: T.C., X.F., X.T., A.J.W., Q.X. Writing—original draft: J.L., T.C. Writing—review & editing: X.F., A.J.W., J.D.J.

Competing interests

The authors declare no competing interests.

Additional information

Supplementary information The online version contains supplementary material available at https://doi.org/10.1038/s41467-026-68341-3.

Correspondence and requests for materials should be addressed to Xuanmei Fan.

Peer review information *Nature Communications* thanks Chris Massey and the other, anonymous, reviewer(s) for their contribution to the peer review of this work. A peer review file is available.